On the existence of self-similar structures in turbulent pipe flow

Leo H. O. Hellström

Dept. of Mech. and Aerospace Engineering
Princeton University, Princeton, NJ
lhellstr@Princeton.EDU

Tyler Van Buren

Dept. of Mech. and Aerospace Engineering
Princeton University, Princeton, NJ
tburen@Princeton.EDU

John C. Vaccaro

Dept. of Engineering
Hofstra University, Hempstead, NY
John.C.Vaccaro@Hofstra.EDU

Alexander J. Smits

Dept. of Mech. and Aerospace Engineering
Princeton University, Princeton, NJ
asmits@Princeton.EDU

Abstract

Townsend's attached eddy hypothesis forms the basis for one of the most far-reaching concepts in the analysis of the logarithmic layer in wall-bounded turbulent flows. The hypothesis proposes that the eddying motions in the inertially dominated region are energetic and geometrically self-similar eddies that scale with the distance from their eddy center to the wall, implying that these three-dimensional eddies can be completely scaled using a single length scale. The attached eddy hypothesis has been used successfully to predict turbulence statistics and the spectral behavior in wall-bounded flows.

Here, we experimentally investigate the existence of self-similar flow structures in fully-developed turbulent pipe flow at $Re_\tau \approx 2390$. The data is simultaneously acquired at two pipe cross-sections using two stereo PIV systems, where the streamwise separation ranges from 0 to $9.97R$. The structures are unconditionally sorted by their spanwise length scale through an azimuthal Fourier decomposition. The sorted structures are thereafter investigated using two-point correlations, and the resulting correlation maps are shown to exhibit self-similar behaviour with respect to its spanwise length scale. This single length scale provides a complete description of the shape of the self-similar eddies.

Introduction

Townsend's attached eddy hypothesis is one of the most important conceptual frameworks to describe the behavior of turbulence in high Reynolds number wall-bounded flows. The hypothesis proposes that the eddying motions in the logarithmic region are attached to the wall, in the sense that they scale with its distance from the wall (Townsend, 1976). The model considers only the energy containing, inertially dominated motions that are independent of viscosity. Townsend further suggested that the eddies, spanning a wide range of sizes, could be linearly superimposed following a probability distribution for each eddy size, such that the model produces a constant shear stress. This model then predicts a logarithmic behavior for both the streamwise and wall-parallel variances, a prediction strongly supported by recent experiments by Hultmark *et al.* (2012) and Marusic *et al.* (2013) and direct numerical simulations (DNS) by Jimenez & Hoyas (2008) and Lee & Moser (2015).

Although these findings on logarithmic scaling implicitly support the attached eddy hypothesis, they do not reveal the nature of the self-similar coherent structures themselves. Because these motions, located in the logarithmic region, constitute the essential elements of the theory, the search for the appropriate description of the self-similar eddying motion is an ongoing quest, which closely follows the search for organized motions in wall-bounded flows. In pursuing this aim, it is crucial to bear in mind that the representative eddy is a statistical concept that does not necessarily reflect the shape or organization of any individual eddy but instead represents the features of an average eddy, or even an assemblage of eddies.

In the search for the representative eddy, Townsend (1976) proposed a double cone vortex which was based on the flow visualizations by Kline *et al.* (1967) and the the POD analysis of pipe flow by Bakewell Jr & Lumley (1967). The identification of the hairpin vortices by Head & Bandyopadhyay (1981) inspired Perry & Chong (1982) and Perry *et al.* (1986) to model the self-similar eddies as lambda-shaped vortex loops. The attached eddy hypothesis is a linear model and does not resolve the non-linear scale interactions. This restriction affects the choice of representative eddy, which needs to be large enough to contain the group of non-linearly interacting scales. To that end, Marusic (2001) and Woodcock & Marusic (2015) used a train of hairpins as the typical representative eddy, inspired by the findings of Head & Bandyopadhyay (1981) and Adrian *et al.* (2000) who showed that hairpin vortices of different size spatially align in the streamwise direction forming a larger coherent entity, the so-called hairpin packet or large-scale motion (LSM). Such model eddies are used to recreate the statistical features of the turbulence, but the physical connection with the turbulent motions themselves is still elusive.

More recently, Hwang (2015) performed a numerical simulation in a channel flow and found that the self-similar structures in the log layer are the most energetic structures, and suggested that the size of each of the attached eddies would be characterized by its spanwise length scale. Hellström *et al.* (2011) and Hellström & Smits (2014) showed that proper orthogonal decomposition (POD) is a useful tool for extracting the large energetic structures in turbulent pipe flow, and that the appropriate decomposition in the spanwise (azimuthal) direction is a Fourier decomposition. Hellström *et al.* (2016) built on this work and and showed that the azimuthal wave length of the POD modes was proportionate to its wall-normal height, providing a statistical structure with self-similar cross-sectional behavior. Here, we expand on this work by simultaneously performing stereo Particle Image Velocimetry (PIV) in two pipe cross-sections using two stereo PIV systems. This allows us to create a statistical picture of the three-dimensional structures, and subsequently address their scaling.

Experimental setup

The experiments were conducted in a $200D$ long pipe facility, consisting of seven glass sections each 1.2 m long with an inner diameter $D = 38.1 \pm 0.025$ mm. The working fluid was water seeded with 10μm glass hollow spheres. The data were simultaneously acquired in two cross-sectional planes using two stereoscopic PIV systems (2D-3C).

The first PIV system remained stationary and consisted of a pair of 5.5 Megapixel LaVision Imager sCMOS cameras arranged vertically above and below the pipe. The second system consisted of a pair of 4.0 Megapixel LaVision Imager SX cameras mounted horizontally on a low friction rail and driven by a traverse for streamwise motion. The mobile system was also equipped with a LaVision articulating light delivery arm, allowing the laser sheet to be moved together with the cameras. The streamwise displacement of the second camera was measured with a dial micrometer with a 12.7μm resolution. In order to reduce the error in the measured distance, the displacement was recorded as the cumulative displacement referenced from the origin. The test section was enclosed by a rectangular acrylic box, filled with water to minimize the optical distortion due to refraction through the pipe wall. An access port was located immediately downstream of the test section in order to insert the stereo PIV calibration target while the pipe was filled with water. The target had 272 dots set in a rectangular grid, and was traversed 2 mm in each direction of the laser sheets, resulting in three calibration images for each stereo PIV camera and system.

The distinction between two laser sheets relies on that the light scattering off the particles is governed by Rayleigh scattering, where the scattered light maintain its polarization. Hence, following the procedure of Hellström *et al.* (2015), the two laser sheets were orthogonally polarized using two independent $\lambda/2$-wave plates and each camera was subsequently equipped with linear polarizers such that particles situated in each system's laser sheet is only visible to that system's cameras.

The Reynolds number, $Re_D = U_b D/\nu = 100\ 000$, where D is the diameter ($= 2R$), U_b is the bulk velocity, and ν is the kinematic viscosity. The corresponding friction Reynolds number is $Re_\tau = u_\tau R/\nu \approx 2390$, where $u_\tau = \sqrt{\tau_w/\rho}$, τ_w is the wall the shear stress, and ρ is the water density. Each data set contains 2000 image pairs and was acquired at $10Hz$, corresponding to an average convective displacement of $13.8R$ between snapshots. All snapshots in the time series can therefore be considered to be statistically independent. A total of 21 data sets were obtained, where the streamwise distance between the two interrogation planes (ξ/R) was logarithmically increasing, such that $(\xi/R) \in \{0.0,\ 0.0262,\ 0.0357,\ 0.0488,\ 0.0672,\ 0.0919,\ 0.126,\ 0.171,\ 0.234,\ 0.320,\ 0.438,\ 0.598,\ 0.818,,\ 1.12,\ 1.53,\ 2.09,\ 2.86,\ 3.90,\ 5.34,\ 7.30,\ 9.97\}$.

Results and Discussion

The current data set allows us to create the normalized three dimensional correlation map, $\rho(m,\xi,\eta)$:

$$\rho(m,\xi,\eta) = \frac{< \int_r \hat{\mathbf{u}}_1(m,r,x_0)\hat{\mathbf{u}}_2^*(m,r+\eta,x_0+\xi)\sqrt{r(r+\eta)}dr >_t}{< \int_r \hat{\mathbf{u}}_1(m,r,x_0)\hat{\mathbf{u}}_2^*(m,r,x_0)rdr >_t} \tag{1}$$

where $\hat{\mathbf{u}} = [\hat{u}_x\ \hat{u}_r\ \hat{u}_\theta]$ represents the azimuthally Fourier transformed velocity field and $*$ represents the conjugate transpose. Subscripts 1 and 2 refer to PIV systems 1 and 2, respectively. It should be noted that the correlation coefficient does not resolve the wall-normal location of a structure, only the extent it remains correlated in the wall-normal direction.

The line plots for correlations where $\eta = 0$ and $m \in [5,\ 40]$ are shown in figure 1. The correlations reveal the streamwise extent of a structure unconditionally sorted by its spanwise wave length

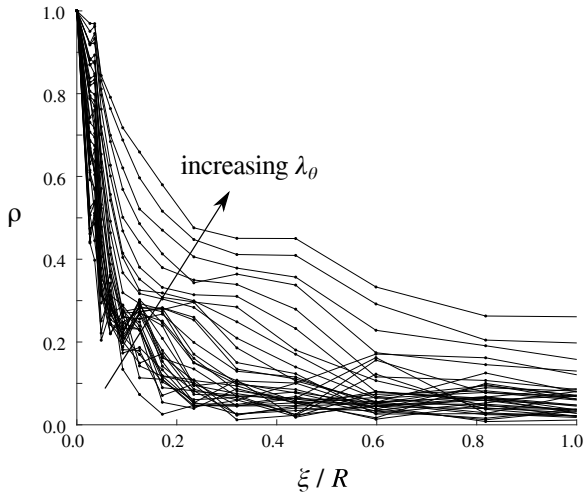

Figure 1. Streamwise correlation $\rho(m,\xi/R,\eta/R=0)$ for $m \in \{5,\ 40\}$.

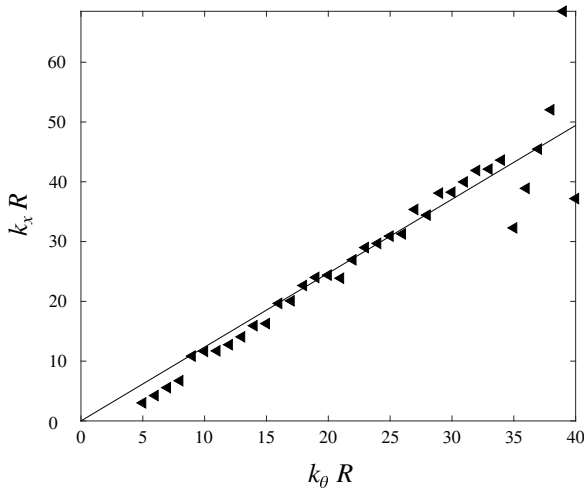

Figure 2. Comparison between the spanwise and streamwise length scales for $m \in [5,\ 40]$. Solid line represents the behaviour of self-similar structures: $k_x = 1.236\ k_\theta$.

$(\lambda_\theta = 2\pi R/m)$, disregarding any wall-normal migrations. It may be seen that the streamwise extent of the correlations decreases with decreasing spanwise wave length (or increasing m). In addition, the correlations show a secondary peak located at $\xi/R \approx 0.43$ for $m = 5$ and $\xi/R \approx 0.12$ for $m = 40$. Because the location of the secondary peak depends on the spanwise wavelength it is a dynamical feature, and not due to a misalignment of the streamwise planes when acquiring the data.

The streamwise wavelength (λ_x) is now estimated by finding the location (ξ/R) where the correlation falls below some defined threshold. Here we chose e^{-2} (0.1353) to represent the decay of the correlation function. This threshold was chosen such that it would encompass the region around the secondary peak.

The relationship between the spanwise wave number $(k_\theta R = 2\pi R/\lambda_\theta = m)$ and streamwise wave number $(k_x R = 2\pi R/\lambda_x)$ is seen in figure 2. A set of self-similar structures are characterized by $k_x \propto k_\theta$ (or $\lambda_x \propto \lambda_\theta$), which is visualized by the solid line in figure 2. The slope depends on the chosen threshold when evaluating λ_x, but for the threshold used here the slope is empirically estimated to be 1.236. The deviations from linearity for the high wave numbers is probably due to the difficulties of accurately estimating the

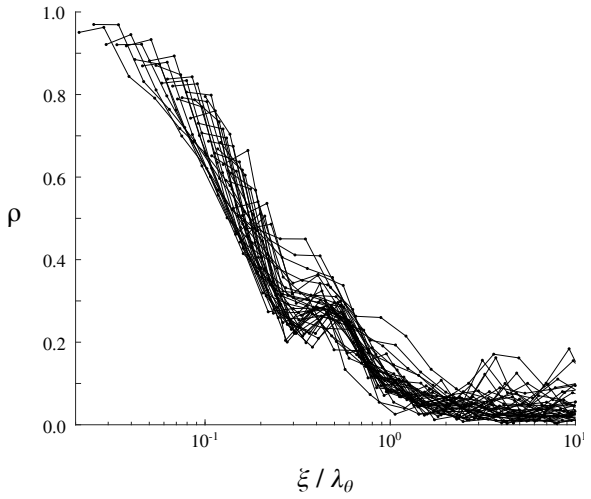

Figure 3. Streamwise correlations in self-similar coordinates. $\rho(m, \xi/\lambda_\theta, \eta/\lambda_\theta = 0)$ for $m \in [5,\ 40]$, where the length scales are normalized with λ_θ.

streamwise wave length for the small structures as the streamwise grid resolution decreases.

Therefore the spanwise and streamwise length scales exhibit a linear relationship for $k_x R \in [3.017,\ 43.62]$, with structure sizes spanning more than an order of magnitude, $\lambda_x/R \in [0.1440,\ 2.083]$, suggesting that the spanwise length scale can be used as a unifying scaling parameter. When the streamwise coordinate is normalized by the spanwise length scale, as in Figure 3, we see that indeed the correlations exhibit a self-similar behaviour. It can also be seen that the region displaying a secondary peak collapses, with the peak centered at $\xi/\lambda_\theta = 0.50$.

The nature of the secondary peak is clearer in the two-dimensional maps, where we show the first quadrant of the correlations ($\xi \geq 0;\ \eta \geq 0$) with respect to wall-normal and streamwise shifts. Figures 4(a-f) shows the correlations for $m \in \{10,\ 20,\ 30,\ 40,\ 55,\ 65\}$, where the spanwise length scale for the structure in figure 4(a) is 6.58 times larger than that in figure 4(f).

The correlation maps are similar for $m \in [5,\ 35]$, after which they expand both in the streamwise and wall-normal directions. Hellström *et al.* (2016) used a POD analysis and found a similar cut-off ($m \in [3,\ 32]$), beyond which the structures could no-longer be considered to be self-similar. The correlation maps reveal a structure with a wall-normal length scale $\mathcal{O}(0.70 - 0.90\lambda_\theta)$ and streamwise length scale $\mathcal{O}(2\lambda_\theta)$, when considering both positive and negative η and ξ. Furthermore, the relationship provided in figure 2 estimates the streamwise end of the structure as $\xi/\lambda_\theta = 0.809$, which is where the correlation falls below e^{-2} along $\eta = 0$.

Within the wave length range $m \in [5,\ 35]$, there exists a secondary peak at $\xi/\lambda_\theta \approx 0.5$, which is most likely the result of the streamwise alignment of structures. This alignment is clearer for the smaller structures, where the intensity of the secondary peak is stronger. The increase in correlation magnitude may indicate a more stable streamwise alignment for the smaller structures; it may equally indicate that the larger structures are less likely to align.

Conclusions

Hellström *et al.* (2016) identified self-similar structures in the cross-sectional plane in a turbulent pipe flow, and found that the wall-normal profile of the structure scaled with its spanwise length scale. They were, however unable to address the streamwise length scale. We have now demonstrated that the streamwise and spanwise length scales are in a constant scale ratio for structures with streamwise length scales spanning more than a decade. Also, the correlation plots were found to be self-similar when scaled by their individual spanwise length-scale, supporting the concept of geometrically self-similar structures existing over a large range of scales.

The streamwise length scale was estimated as the location where the correlation is less than e^{-2}. However, it was shown that there is an alignment of structures within this streamwise region and the lengthscale is therefore based on a train of structures. Because the location of the secondary peak is fixed at $\xi/\lambda_\theta \approx 0.50$ the inclusion of the aligned structures when estimating the streamwise length scale will not affect the self-similarity.

Future work will include a structure analysis incorporating both streamwise extent and wall-normal location of the structures, defined by their azimuthal wave length, and address the origin of the secondary peak.

Acknowledgement

This work was supported under ONR grant no. N00014-15-1-2402 (Program Manager Ron Joslin, Program Director Tom Fu).

REFERENCES

Adrian, R. J., Meinhart, C. D. & Tomkins, C. D. 2000 Vortex organization in the outer region of the turbulent boundary layer. *J. Fluid Mech.* **422**, 1–54.

Bakewell Jr, Henry P & Lumley, John L 1967 Viscous sublayer and adjacent wall region in turbulent pipe flow. *Phys. Fluids* **10** (9), 1880–1889.

Head, M. R. & Bandyopadhyay, P. 1981 New aspects of turbulent boundary-layer structure. *J. Fluid Mech.* **107**, 297–338.

Hellström, L. H. O., Ganapathisubramani, B. & Smits, A. J. 2015 The evolution of large-scale motions in turbulent pipe flow. *J. Fluid Mech.* **779**, 701–715.

Hellström, L. H. O., Marusic, I. & Smits, A. J. 2016 Self-similarity of the large-scale motions in turbulent pipe flow. *J. Fluid Mech.* **792**, R1 (12 pages).

Hellström, L. H. O., Sinha, A. & Smits, A. J. 2011 Visualizing the very-large-scale motions in turbulent pipe flow. *Phys. Fluids* **23**, 011703.

Hellström, L. H. O. & Smits, A. J. 2014 The energetic motions in turbulent pipe flow. *Phys. Fluids* **26** (12), 125102.

Hultmark, M., Vallikivi, M., Bailey, S. C. C. & Smits, A. J. 2012 Turbulent pipe flow at extreme Reynolds numbers. *Phys. Rev. Lett.* **108** (9), 094501.

Hwang, Y. 2015 Statistical structure of self-sustaining attached eddies in turbulent channel flow. *J. Fluid Mech.* **767**, 254–289.

Jimenez, J. & Hoyas, S. 2008 Turbulent fluctuations above the buffer layer of wall-bounded flows. *J. Fluid Mech.* **611**, 215–236.

Kline, S. J., Reynolds, W. C., Schraub, F. A. & Runstadler, P. W. 1967 The structure of turbulent boundary layers. *J. Fluid Mech.* **30** (04), 741–773.

Lee, M. & Moser, R. D. 2015 Direct numerical simulation of turbulent channel flow up to $Re_\tau = 5200$. *J. Fluid Mech.* **774**, 395–415.

Marusic, I. 2001 On the role of large-scale structures in wall turbulence. *Phys. Fluids* **13** (3), 735–743.

Marusic, I., Monty, J. P., Hultmark, M. & Smits, A. J. 2013 On the logarithmic region in wall turbulence. *J. Fluid Mech.* **716**, R3.

Perry, A. E. & Chong, M. S. 1982 On the mechanism of wall turbulence. *J. Fluid Mech.* **119**, 173–217.

Perry, A. E., Henbest, S. & Chong, M. S. 1986 A theoretical and experimental study of wall turbulence. *J. Fluid Mech.* **165**, 163–199.

Townsend, A. A. 1976 *The structure of turbulent shear flow*. Cambridge university press.

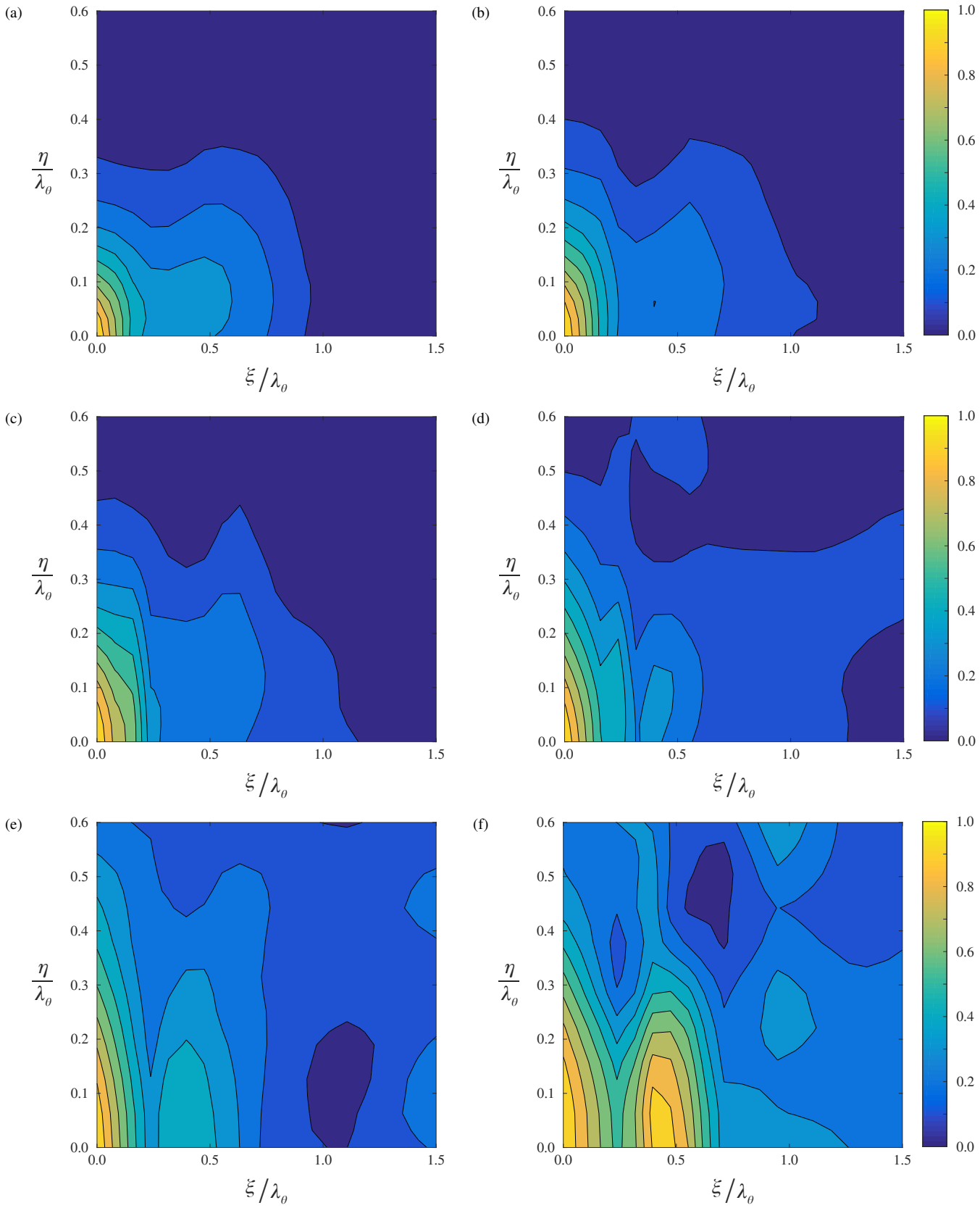

Figure 4. Correlation map of $\rho(m, \xi/\lambda_\theta, \eta/\lambda_\theta)$, where $\lambda_\theta = 2\pi/m$. (a) $m = 10$; (b) $m = 20$; (c) $m = 30$; (d) $m = 40$; (e) $m = 55$; (f) $m = 65$.

Woodcock, J. D. & Marusic, I. 2015 The statistical behaviour of attached eddies. *Phys. Fluids* **27** (1), 015104.